The Astronomical Journal, 157:80 (10pp), 2019 February https://doi.org/10.3847/1538-3881/aaf96a

Late Delivery of Nitrogen to the Earth

Cheng Chen, Jeremy L. Smallwood, Rebecca G. Martin, and Mario Livio
Department of Physics and Astronomy, University of Nevada, Las Vegas, 4505 S. Maryland Parkway, Box 454002, Las Vegas, NV 89154, USA
chenc21@unlv.nevada.edu
Received 2018 October 19; revised 2018 December 14; accepted 2018 December 16; published 2019 January 28

Abstract

Atmospheric nitrogen may be a necessary ingredient for the habitability of a planet as its presence helps to prevent water loss from a planet. The present-day nitrogen isotopic ratio, $^{15}N/^{14}N$, in the Earth's atmosphere is a combination of the primitive Earth's ratio and the ratio that might have been delivered in comets and asteroids. Asteroids have a nitrogen isotopic ratio that is close to the Earth's. This indicates either a similar formation environment to the Earth or that the main source of nitrogen was delivery by asteroids. However, according to geological records, the Earth's atmosphere could have been enriched in ^{15}N during the Archean era. Comets have a higher $^{15}N/^{14}N$ ratio than the current atmosphere of the Earth, and we find that about 5% $\sim$ 10% of nitrogen in the atmosphere of the Earth may have been delivered by comets to explain the current atmosphere of the Earth or the enriched ^{15}N atmosphere of the Earth. We model the evolution of the radii of the snow lines of molecular nitrogen and ammonia in a protoplanetary disk and find that both have radii that put them farther from the Sun than the main asteroid belt. With an analytic secular resonance model and *N*-body simulations we find that the ν_8 apsidal precession secular resonance with Neptune, which is located in the Kuiper Belt, is a likely origin for the nitrogen-delivering comets that impact the Earth.

Key words: accretion, accretion disks – comets: general – Kuiper belt: general

1. Introduction

Nitrogen may be an essential part of an atmosphere for a planet to be habitable (e.g., Stüeken et al. 2016). Nitrogen is a component of chemical compounds that are necessary for growth and reproduction of all animal and plant life on Earth. It is found in amino acids that make up proteins as well as in nitrogenous bases in nucleic acids that store, transcribe, and translate the genetic code. Furthermore, nitrogen influences the surface temperature and water content of the atmosphere, both of which affect planet habitability. The nitrogen content in the atmosphere plays a significant role in the rate of water loss from a planet (e.g., Wordsworth & Pierrehumbert 2013, 2014). If the nitrogen level is too low, water loss may be very efficient for all surface temperatures.

Nitrogen is the most abundant molecule in the atmosphere of the Earth, comprising about 78% of our atmosphere by volume, but still, its origin is not well understood. The reservoir of nitrogen in the crust and the mantle of the Earth currently is thought to be between 0.4 and 7 times the present-day atmospheric amount (e.g., Marty 1995; Halliday 2013; Johnson & Goldblatt 2015). Isotopic measurements suggest that most of the current atmospheric nitrogen is from the inner solar system (Füri & Marty 2015). The relative abundance of the two isotopes of nitrogen $^{15}N/^{14}N$ in the Earth is similar to Venus, Mars, and primitive meteorites such as chondrites (e.g., Hutsemékers et al. 2009; Marty 2012; Bergin et al. 2015; Harries et al. 2015).

In the case of the Earth we know that most of the nitrogen was accreted locally. However, this may not be universally the case. Therefore, a study of potential habitability (assuming that nitrogen is a necessary ingredient) needs to explore other potential delivery mechanisms.

The isotopic ratio of nitrogen in the present-day atmosphere is measured to be $^{15}N/^{14}N = 3.676 \times 10^{-3}$ (Junk & Svec 1958). However, the Earth's mantle is relatively depleted in ^{15}N compared to the Earth's atmosphere. We compare the ratios with

$$\delta^{15}N = \left(\frac{(^{15}N/^{14}N)_{\rm mantle}}{(^{15}N/^{14}N)_{\rm atmosphere}} - 1 \right) \times 1000. \quad (1)$$

In the Earth's mantle, $\delta^{15}N$ is estimated to be in the range of -5 ‰ to -30‰ (Cartigny & Marty 2013). Thus, the isotopic ratio of nitrogen in the Earth's mantle is in the range between $^{15}N/^{14}N = 3.566 \times 10^{-3}$ and 3.658×10^{-3} (Javoy et al. 1986; Murty & Mohapatra 1997; Cartigny et al. 1998; Marty & Zimmermann 1999; Jia & Kerrich 2004; Cartigny & Marty 2013). Moreover, according to the record of Archean sedimentary rocks and crustal hydrothermal systems, the Earth may have had a ^{15}N-enriched atmosphere with $\delta^{15}N = 30$‰ and $^{15}N/^{14}N = 3.786 \times 10^{-3}$ in the Archean eon (Jia & Kerrich 2004), 4–2.5 billion years ago. This high estimate was later questioned because it was based on the analysis of metamorphosed crustal rocks (Papineau et al. 2005; Ader et al. 2006; Stüeken et al. 2015). Different geological records of less metamorphosed Archean sedimentary rocks suggest a lower value $\delta^{15}N$ in the range of 0‰ to 15‰ (Sano & Pillinger 1990; Pinti et al. 2001), and more recent estimates based on the analysis of fluid inclusions having trapped Archean seawater concluded that the N isotope composition of the Archean atmosphere was close to 0‰ (Marty et al. 2013; Avice et al. 2018). In our calculations (see Section 3), we consider both a ^{15}N-rich atmosphere and the present-day atmosphere.

Several possible mechanisms may explain a high value of $^{15}N/^{14}N$ during the Archean era, such as hydrodynamic escape of light isotopes or heterogeneous accretion of the Earth that forms from material with ^{15}N depleted and then accretes a late veneer composed of chondritic material and a minor contribution of ^{15}N-enriched comets. However, these mechanisms are difficult to quantify (Javoy 1998; Marty 2012; Cartigny & Marty 2013). It is most likely that to reach the current nitrogen

isotopic ratio of the Earth's atmosphere or the ^{15}N-enriched atmosphere in the Archean era, there must have been some comets delivered to the Earth after the Earth formed and differentiated (Jia & Kerrich 2004; Rice et al. 2018).

Enstatite chondrites formed in the inner solar system and could be the primary ingredient to form terrestrial planets (Wasson & Kallemeyn 1988). These chondrites can carry nitrogen in osbornite, sinoite, and nierite (Rubin & Choi 2009). On the other hand, nitrogen was probably delivered to the Earth by comets in the form of ammonia ices or simple organic compounds such as HCN. In laboratory studies, molecular nitrogen can be trapped and released by amorphous ice (Bar-Nun et al. 1988). Although in the case of Halley's comet, only a small amount of N_2^+ was detected due to the enrichment of CO over N_2 in amorphous ice (Notesco & Bar-Nun 1996). The abundance of nitrogen in the surface layer of a comet measured by a satellite does not necessarily represent the ratio in its nucleus (Prialnik & Bar-Nun 1992). In the case of Halley's comet, most of the nitrogen is in the form of compounds (Geiss 1987, 1988; Krankowsky 1991; Meier et al. 1994). The amount of nitrogen that can be trapped in ice at temperatures of around 30 K is five orders of magnitude higher than in ice at a temperature of 100 K (Bar-Nun et al. 1988). However, in comets, noble gases have about an equal abundance as molecular nitrogen. If these were delivered to the Earth, the Earth would have had an overabundance of noble gases (Owen & Bar-Nun 1995; Marty et al. 2017). Nevertheless, a recent analysis from the Rosetta Orbiter Spectrometer for Ion and Neutral Analysis (ROSINA) revealed that the relative abundance of Ar/N_2 inside the icy nucleus of the 67P/Churyumov–Gerasimenko is $9.1 \pm 0.3 \times 10^{-3}$ (Balsiger et al. 2015). Therefore, comets may not contain the same amount of noble gases as they do nitrogen. Moreover, the xenon isotopic composition shows a deficit in heavy xenon isotopes from ROSINA. By considering that the origin of a primordial atmospheric xenon component is a mixture of chondritic and cometary xenon, the present Earth's atmosphere contains $22 \pm 5\%$ cometary xenon (Marty et al. 2017).

The nitrogen isotopic ratio could change in the outer regions of the solar system where comets formed at extremely low temperature. Large enhancements of the isotopic ratio $^{15}N/^{14}N$ can occur in cold, dense gas where CO is frozen out. In particular, if the temperature is around 7–10 K, then the upper layers of the grains can be enhanced in ^{15}N by up to an order of magnitude (Rodgers & Charnley 2008). This mechanism introduces an uncertain factor in the measured $^{15}N/^{14}N$ isotopic ratio in comets. Some comets have an anomalous nitrogen isotopic ratio that is about twice the terrestrial ratio (Manfroid et al. 2009).

In this work, we explore the possibility of late delivery for the ^{15}N-enriched nitrogen in the atmosphere of the Earth. In Section 2, we examine the evolution of a protoplanetary disk in which planetesimals later form. We calculate the location of the ammonia and nitrogen snow lines—the radius outside of which each would have condensed out of the gas and would have been incorporated into the solid bodies. While there is evidence that most of the nitrogen was delivered locally it is still interesting to explore whether some of it could be delivered at late times, via comets or asteroids. In Section 3, we consider what isotopic nitrogen ratios tell us about how much of the nitrogen could have been delivered by comets, and find that it could have been a significant fraction. In Section 4, we examine possible delivery mechanisms to the Earth for the relevant solid bodies. In particular, we show how comets are perturbed by mean motion and secular resonances with the planets in the solar system, and we use *N*-body simulations to show that resonances can play a role in the delivery of comets to the Earth. Finally, we draw our conclusions in Section 5.

2. Protoplanetary Disk Evolution

The temperature of a protoplanetary disk generally decreases with distance from the central star. A snow line marks the radial distance from the star outside of which the temperature drops below the condensation temperature of a particular compound. The condensation temperature for hydrated ammonia is about $T_{\rm snow,NH_3} = 131$ K and for hydrated nitrogen is about $T_{\rm snow,N_2} = 58$ K (Lodders 2003). In this section, we consider the evolution of these snow lines in a protoplanetary disk. The snow lines determine where ammonia and nitrogen were incorporated in a solid form into planetesimals that formed there.

Material in the disk interacts through viscosity that is thought to be driven by the magnetorotational instability (MRI) that drives turbulence in the disk (Balbus & Hawley 1991). We first consider the snow line radii in a steady-state fully turbulent disk model. However, protoplanetary disks are thought to contain a region of low turbulence at the disk midplane, known as a "dead zone," where the disk is not sufficiently ionized for the MRI to operate (e.g., Gammie 1996; Gammie & Menou 1998). Thus, we also consider how the presence of a dead zone affects the evolution of the snow lines. We follow Martin & Livio (2014) and derive analytic solutions for the snow line radii in each case.

2.1. A Fully Turbulent MRI Disk

Material in an accretion disk orbits the central star of mass, $M_\star$, with Keplerian velocity at radius R with angular velocity $\Omega = \sqrt{GM_\star/R^3}$ (Pringle 1981). The viscosity in a fully MRI turbulent disk is

$$\nu = \alpha_{\rm m}\frac{c_{\rm s}^2}{\Omega}, \tag{2}$$

where $\alpha_{\rm m}$ is the viscosity parameter (Shakura & Sunyaev 1973) and the sound speed is $c_{\rm s} = \sqrt{\mathcal{R}T_{\rm c}/\mu}$, where $\mathcal{R}$ is the gas constant, μ is the gas mean molecular weight, and $T_{\rm c}$ is the midplane temperature. With a constant accretion rate, $\dot{M}$, through all radii, the surface density of a steady-state disk is

$$\Sigma = \frac{\dot{M}}{3\pi\nu} \tag{3}$$

(Pringle 1981). The surface temperature is determined through the balance of heating from viscous effects and irradiation from the central star

$$\sigma T_{\rm e}^4 = \frac{9}{8}\frac{\dot{M}}{3\pi}\Omega^2 + \sigma T_{\rm irr}^4 \tag{4}$$

(e.g., Cannizzo 1993; Pringle et al. 1986), where σ is the Stefan–Boltzmann constant and the irradiation temperature is

$$T_{\rm irr} = \left(\frac{2}{3\pi}\right)^{\frac{1}{4}}\left(\frac{R_\star}{R}\right)^{\frac{3}{4}}T_\star \tag{5}$$

(Chiang & Goldreich 1997), where $T_\star$ is the temperature and $R_\star$ is the radius of the star. The midplane temperature is related to the surface temperature through

$$T_c^4 = \tau T_e^4, \tag{6}$$

where the optical depth, τ, is given by

$$\tau = \frac{3}{8}\kappa\frac{\Sigma}{2} \tag{7}$$

and the opacity is $\kappa = aT_c^b$. In our model, we take $a = 0.0001$ and $b = 2.1$ as dust dominates the absorption properties of matter in the disk (Armitage et al. 2001).

The snow line radius in the disk is found by solving $T_c = T_{\rm snow}$. In our model, we assume $M_\star = 1\,M_\odot$, $R_\star = 3\,R_\odot$, and $T_\star = 4000$ K. There remains some uncertainty in the value of the viscosity parameter (e.g., King et al. 2007). Observations of FU Ori show $\alpha_{\rm m} \approx 0.01$ (Zhu et al. 2007), while from observations of X-ray binaries and cataclysmic variables, it is estimated that $\alpha_{\rm m} \approx 0.1 \sim 0.4$ (King et al. 2007). Since we consider young stellar objects, we assume that $\alpha_{\rm m} = 0.01$ in a fully turbulent MRI disk.

We adapt the approximate analytical steady-state solution of the CO snow line in Martin & Livio (2014) and find analytic fits to the nitrogen snow line radius

$$R_{\rm N_2,snow} \approx 3.6\left(\frac{\alpha_{\rm m}}{0.01}\right)^{-\frac{2}{9}}\left(\frac{M_\star}{M_\odot}\right)^{\frac{1}{9}}\left(\frac{\dot{M}}{10^{-8}\,M_\odot\ {\rm yr}^{-1}}\right)^{\frac{2}{9}} \times \left(\frac{T_{\rm N_2,snow}}{58\ {\rm K}}\right)^{-0.64}\left(\frac{R_\star}{3\,R_\odot}\right)^{\frac{2}{3}}\left(\frac{T_\star}{4000\ {\rm K}}\right)^{\frac{8}{9}}{\rm au} \tag{8}$$

and the ammonia snow line radius

$$R_{\rm NH_3,snow} \approx 2.1\left(\frac{\alpha_{\rm m}}{0.01}\right)^{-\frac{2}{9}}\left(\frac{M_\star}{M_\odot}\right)^{\frac{1}{9}}\left(\frac{\dot{M}}{10^{-8}\,M_\odot\ {\rm yr}^{-1}}\right)^{\frac{2}{9}} \times \left(\frac{T_{\rm NH_3,snow}}{131\ {\rm K}}\right)^{-0.64}\left(\frac{R_\star}{3\,R_\odot}\right)^{\frac{2}{3}}\left(\frac{T_\star}{4000\ {\rm K}}\right)^{\frac{8}{9}}{\rm au}. \tag{9}$$

These are valid for relatively low accretion rates, $\dot{M} \lesssim 10^{-8}\,M_\odot\ {\rm yr}^{-1}$, where irradiation dominates the viscous heating term.

The numerical values of the snow line radii in Equations (8) and (9), for the standard parameters chosen, are uncomfortably small. The ammonia snow line lies inside of the main asteroid belt, while the nitrogen snow line lies within it. Figure 1 shows the full numerical solution for the snow line radii for nitrogen and ammonia in a fully turbulent disk as a function of the steady-state accretion rate (dashed lines) found by solving $T_c = T_{\rm snow}$ along with Equations (4)–(6). This exposes the problem with fully turbulent disks, in that the snow line moves in too close to the host star during the low accretion rate phase when the disk is near the end of its lifetime (Garaud & Lin 2007; Martin & Lubow 2011; Oka et al. 2011; Martin & Livio 2014). This contradicts observations of the composition of asteroids in the asteroid belt (e.g., DeMeo & Carry 2014). To explore possible solutions to this problem, we consider a more realistic disk—one with a dead zone—in the following section.

The dashed lines in Figure 2 show the surface density at the snow line radius as a function of the accretion rate. For low accretion rates, the surface density at the snow line radius becomes very small, $\Sigma \lesssim 10$ g cm^{-2}. Assuming a gas to solid ratio of 100 (e.g., Bohlin et al. 1978; Hayashi 1981), the surface density of solid material is $\lesssim$0.1 g cm^{-2}. In the fully turbulent disk model there is little solid material available for planetesimal formation in the outer parts of the disk.

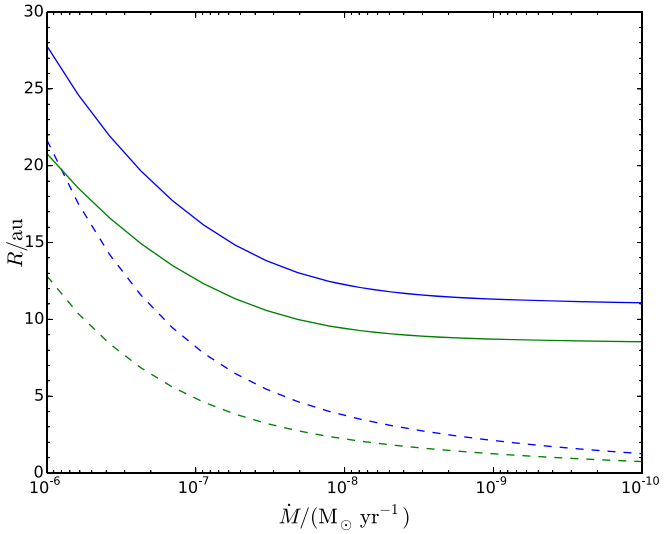

Figure 1. Nitrogen (blue) and ammonia (green) snow lines as a function of accretion rate in a steady-state disk with $M_\star = M_\odot$, $T_\star = 4000$ K, $R_\star = 3\,R_\odot$, $T_{\rm N_2,snow} = 58$ K, and $T_{\rm NH_3,snow} = 131$ K. The dashed lines show the snow lines with the fully MRI turbulent disk with $\alpha_{\rm m} = 0.01$. The solid lines represent the snow lines in a disk in a self-gravitating dead zone.

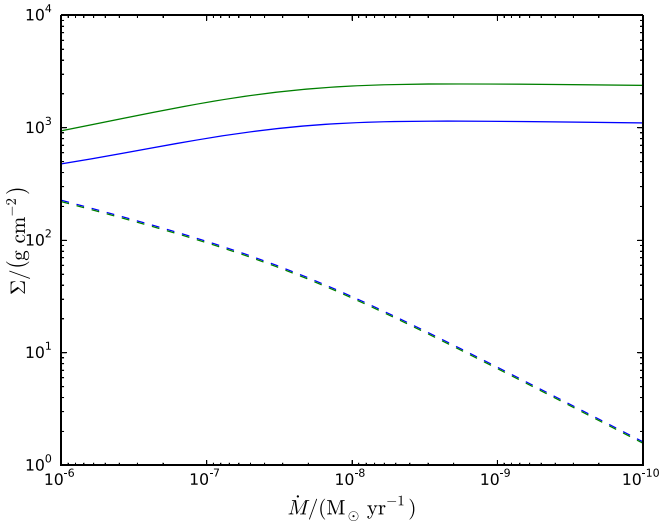

Figure 2. Surface density at the snow line radius, $R = R_{\rm snow}$, in the steady-state disk for the nitrogen snow line radius (blue lines) and the ammonia snow line radius (green lines). The solid lines are disks with self-gravitating dead zones, and the dashed lines, which lie on top of each other, are fully MRI turbulent disks with $\alpha_{\rm m} = 0.01$.

2.2. A Disk with a Dead Zone

The MRI requires a sufficiently high level of ionization in the disk for it to operate. The inner regions of a protoplanetary disk are hot enough to be thermally ionized where $T_c \geqslant T_{\rm crit}$. The critical temperature, $T_{\rm crit}$, is thought to be around 800 K for activating the MRI (Umebayashi & Nakano 1988). However, farther from the host star, external sources such as cosmic rays and X-rays from the central star ionize only the surface layers up to a critical surface density, $\Sigma_{\rm crit}$. The value of the critical surface density is not well determined (Martin et al. 2012a, 2012b). For

T Tauri stars, cosmic rays ionize a critical surface density of $\Sigma_{\rm crit} \approx 100$ g cm^2 (Gammie 1996). However, this value could be much lower if we consider the chemical reaction of charged particles (Sano et al. 2000). Bai & Goodman (2009) and Turner & Sano (2008) found that the MRI could operate in the surface layer of a disk ionized by stellar X-rays with $\Sigma_{\rm crit} \approx$ 1–30 g cm^{-2}. Where the surface density is larger than this, $\Sigma \geqslant \Sigma_{\rm crit}$, a dead zone forms at the disk midplane where the MRI cannot operate (e.g., Gammie 1996; Gammie & Menou 1998).

In the dead zone layer, material builds up due to the lower viscosity and the small mass transport rate. The disk becomes self-gravitating when the Toomre (1964) parameter, $Q = c_{\rm s}\,\Omega/\,\pi G\Sigma$, is less than the critical, $Q_{\rm crit} = 2$. Then, a second type of turbulence, gravitational turbulence, is driven, with a viscosity given by

$$\nu_{\rm g} = \alpha_{\rm g}\frac{c_{\rm g}^2}{\Omega}, \tag{10}$$

and the alpha parameter is

$$\alpha_{\rm g} = \alpha_{\rm m}\exp(-Q^4) \tag{11}$$

(e.g., Zhu et al. 2010). The disk can reach a steady state with a self-gravitating dead zone (e.g., Martin & Lubow 2013, 2014; Rafikov 2015). Martin & Livio (2012) found that the evolution of the snow line is significantly altered in a time-dependent disk with a dead zone compared with a fully turbulent disk model. The build up of material can lead to the disk being gravo-magneto unstable (see the disk structure sketches in Martin & Livio 2013). The temperature in the dead zone increases sufficiently for the MRI to be triggered there, leading to an accretion outburst. However, the outer parts of the disk that we are interested in here remain in a steady state. Thus, we consider only steady-state self-gravitating disk solutions in this work.

We follow Martin & Livio (2012) to obtain an analytic solution for the snow line radii assuming that both the ammonia and nitrogen snow lines are in the self-gravitating part of the dead zone. The disk has MRI active layers over a self-gravitating dead zone, but we assume that $\Sigma \gg \Sigma_{\rm crit} \approx 0$. The self-gravitating disk has a surface density

$$\Sigma = \frac{c_{\rm g}\Omega}{\pi G Q}. \tag{12}$$

The accretion rate of the steady disk is

$$\dot{M} = 3\pi\nu_{\rm g}\Sigma = \left(\frac{3c_{\rm g}^3\alpha_{\rm m}}{G}\right)\frac{\exp(-Q^4)}{Q}. \tag{13}$$

The term in brackets is constant for a fixed snow line temperature. This expression depends sensitively on Q, but Q is approximately constant in the range of accretion rates we use. We scale the variables to $T'_{\rm N_2,snow} = T_{\rm N_2,snow}/58$ K, $T'_{\rm NH_3,snow} = T_{\rm NH_3,snow}/131$ K, $\alpha'_{\rm m} = \alpha_{\rm m}/0.01$, $M'_\star = M_\star/M_\odot$, $R'_\star = R_\star/3\,R_\odot$, and $R' = R/$au. Then, we can solve Equation (13) to calculate the scaled Toomre parameter

$$Q' = \frac{Q}{Q_{\rm crit}} = 0.69\left[\frac{W(x)}{W(x_0)}\right]^{\frac{1}{4}}, \tag{14}$$

where we define

$$x_{\rm N_2} = x_{0,\rm N_2}\frac{\alpha'^4_{\rm m}T'^6_{\rm N_2,snow}}{M'^4_\star} \tag{15}$$

with $x_{0,\rm N_2} = 3.86 \times 10^{10}$ and

$$x_{\rm NH_3} = x_{0,\rm NH_3}\frac{\alpha'^4_{\rm m}T'^6_{\rm NH_3,snow}}{M'^4_\star} \tag{16}$$

with $x_{0,\rm NH_3} = 5.13 \times 10^{12}$. The equation

$$x = W(x)\exp[W(x)] \tag{17}$$

defines the Lambert function, W.

The steady-state energy equation of a disk with a self-gravitating dead zone is

$$\sigma T_{\rm e}^4 = \frac{9}{8}\nu_{\rm g}\Sigma\Omega^2 + \sigma T_{\rm irr}^4. \tag{18}$$

The midplane temperature of the disk is related to the disk surface temperature with Equations (5)–(7). In Figure 1, the two solid lines show the snow line radii that are the solutions to $T_{\rm c} = T_{\rm snow}$ with Equation (18). The snow line radius in the disk model with a dead zone is farther from the central star than in the fully turbulent disk model because the temperature of the disk is higher. With a dead zone, for low accretion rates the snow line radius is insensitive to the accretion rate. The self-gravitating dead zone prevents the snow lines from moving too close to the central star in the late stages of disk evolution.

For lower accretion rates ($\dot{M} \leqslant 10^{-8}\,M_\odot$ yr^{-1}), irradiation dominates over the viscous heating term, and we approximate Equation (18) with $T_{\rm e} = T_{\rm irr}$ and find the analytic snow line radius for nitrogen to be

$$R_{\rm N_2,snow} = 12.6\,M'^{\frac{1}{9}}_\star R'^{\frac{2}{3}}_\star T'^{\frac{8}{9}}_\star T'^{-0.31}_{\rm N_2,snow}\left[\frac{W(x)}{W(x_0)}\right]^{-\frac{1}{18}}\ \text{au} \tag{19}$$

and for ammonia to be

$$R_{\rm NH_3,snow} = 9.8\,M'^{\frac{1}{9}}_\star R'^{\frac{2}{3}}_\star T'^{\frac{8}{9}}_\star T'^{-0.31}_{\rm NH_3,snow}\left[\frac{W(x)}{W(x_0)}\right]^{-\frac{1}{18}}\ \text{au}. \tag{20}$$

These values are given approximately by

$$R_{\rm N_2,snow} = 12.6\left(\frac{M_\star}{M_\odot}\right)^{\frac{1}{9}}\left(\frac{R_\star}{3\,R_\odot}\right)^{\frac{2}{3}}\left(\frac{T_\star}{4000\ \text{K}}\right)^{\frac{8}{9}} \times\left(\frac{T_{\rm N_2,snow}}{58\ \text{K}}\right)^{-0.31}\ \text{au} \tag{21}$$

and

$$R_{\rm NH_3,snow} = 9.8\left(\frac{M_\star}{M_\odot}\right)^{\frac{1}{9}}\left(\frac{R_\star}{3\,R_\odot}\right)^{\frac{2}{3}}\left(\frac{T_\star}{4000\ \text{K}}\right)^{\frac{8}{9}} \times\left(\frac{T_{\rm NH_3,snow}}{131\ \text{K}}\right)^{-0.31}\ \text{au}. \tag{22}$$

The numerical values of Equations (21) and (22) for our standard parameters are consistent with the solid lines in Figure 1 at low accretion rates.

The solid lines in Figure 2 show the surface density of the disk with a self-gravitating dead zone at the snow line radius, for nitrogen (blue line) and for ammonia (green line). The disk

with the dead zone has a roughly constant surface density with accretion rate, particularly for low accretion rates. The surface density is much higher than even the maximum possible value for the critical surface density that may be MRI active, $\Sigma_{\rm crit} \approx 200\ {\rm g\ cm^{-2}}$. Thus, our assumption of $\Sigma \gg \Sigma_{\rm crit}$ is justified. Furthermore, the surface density at the snow line radii is significantly higher in a disk with a dead zone, thus allowing for more solid bodies to form.

For the low accretion rates expected at the end of the disk lifetime, the snow line radii for nitrogen and ammonia in the solar system are both farther from the Sun than the main asteroid belt. The ammonia snow line lies at about 9 au, while the nitrogen snow line is at 12 au. Thus, comets in the Kuiper Belt are expected to form with significantly more nitrogen than asteroids in the main asteroid belt. In the next section, we consider observational constraints from the isotopic ratio of nitrogen and estimate the fraction of the present Earth's atmosphere that could have been delivered by comets.

3. The Delivery of Cometary Nitrogen to Earth

For the Earth's atmosphere, the present ratio of $^{15}{\rm N}/^{14}{\rm N}$ is the combined result of the isotopic ratio of the primitive Earth's atmosphere, of asteroids, and of comets. We follow the model of Hutsemékers et al. (2009) to find the percentage of nitrogen that may have been brought to Earth by comets.

The isotopic ratio in the present atmosphere is measured to be $(^{15}{\rm N}/^{14}{\rm N})_{\rm t} = 3.676 \times 10^{-3}$ (Junk & Svec 1958). In contrast, the isotopic ratio of the primitive Earth, $(^{15}{\rm N}/^{14}{\rm N})_{\rm p}$, is uncertain. Based on the value of the ratio in enstatite chondrite-type material and measurement of the Earth's interior, we shall therefore consider the isotopic ratio of the primitive Earth's atmosphere $(^{15}{\rm N}/^{14}{\rm N})_{\rm p}$ to be 3.55×10^{-3}, which reflects the ingredients of the Earth in the protosolar nebula (Javoy et al. 1986; Murty & Mohapatra 1997; Cartigny et al. 1998; Marty & Zimmermann 1999; Jia & Kerrich 2004; Cartigny & Marty 2013).

The nitrogen isotopic ratio of the primitive Earth is very similar to that observed in asteroids, thus we consider the nitrogen isotopic ratio of the present Earth as a mixture of that from comets and that from the primitive Earth's atmosphere. The abundances of each isotope are equal to the sum of that in comets and that in the primitive Earth so that

$$n_{\rm p}(^{14}{\rm N}) + n_{\rm c}(^{14}{\rm N}) = n_{\rm t}(^{14}{\rm N}) \tag{23}$$

and

$$n_{\rm p}(^{15}{\rm N}) + n_{\rm c}(^{15}{\rm N}) = n_{\rm t}(^{15}{\rm N}), \tag{24}$$

where n is the abundance and the subscripts p, c, and t represent the primitive Earth, comets, and present Earth, respectively. The terrestrial isotopic ratio weighted by the relative abundances of nitrogen from comets and from the primitive Earth is

$$(^{15}{\rm N}/^{14}{\rm N})_{\rm t} = \frac{n_{\rm c}(^{14}{\rm N})}{n_{\rm t}(^{14}{\rm N})}(^{15}{\rm N}/^{14}{\rm N})_{\rm c} + \frac{n_{\rm p}(^{14}{\rm N})}{n_{\rm t}(^{14}{\rm N})}(^{15}{\rm N}/^{14}{\rm N})_{\rm p}. \tag{25}$$

Combining this with Equation (23) gives the fraction of the abundance of ^{14}N in comets to the total abundance

$$\frac{n_{\rm c}(^{14}{\rm N})}{n_{\rm t}(^{14}{\rm N})} = \frac{(^{15}{\rm N}/^{14}{\rm N})_{\rm p} - (^{15}{\rm N}/^{14}{\rm N})_{\rm t}}{(^{15}{\rm N}/^{14}{\rm N})_{\rm p} - (^{15}{\rm N}/^{14}{\rm N})_{\rm c}}. \tag{26}$$

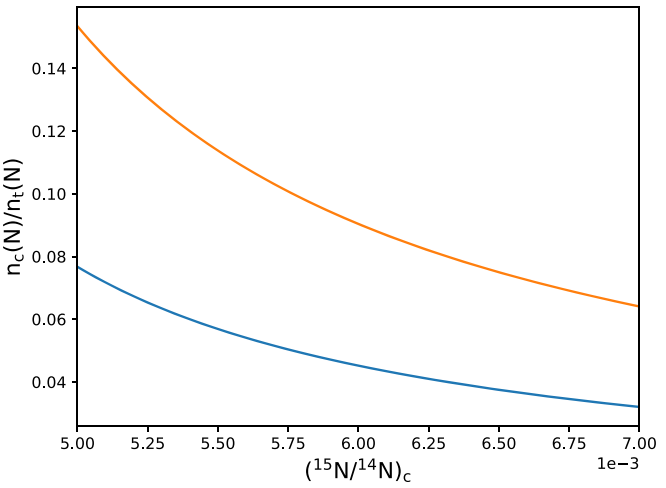

Figure 3. Fraction of the present Earth's nitrogen that was delivered by comets, $n_{\rm c}({\rm N})/n_{\rm t}({\rm N})$, as a function of the cometary isotopic nitrogen ratio, $(^{15}{\rm N}/^{14}{\rm N})_{\rm c}$. The blue line is the model with the primitive Earth ratio of $(^{15}{\rm N}/^{14}{\rm N})_{\rm p} = 3.676 \times 10^{-3}$, and the yellow line is the model with $(^{15}{\rm N}/^{14}{\rm N})_{\rm p} = 3.786 \times 10^{-3}$.

This is the fraction of the nitrogen that was delivered to the Earth by comets compared to the total amount of nitrogen in the atmosphere (Hutsemékers et al. 2009).

The isotopic ratio of nitrogen in comets is uncertain. McKeegan et al. (2006) analyzed COMET 81P/Wild2 grains returned by Stardust and found a bulk isotopic ratio that is close to the terrestrial and chondritic value $(^{15}{\rm N}/^{14}{\rm N})_{\rm c} = 3.55 \times 10^{-3}$, but most comets have a higher value. For comets measured remotely using optical–UV spectroscopy of CN and radio observations of HCN, the isotopic ratio of nitrogen was found to be in the range of $(^{15}{\rm N}/^{14}{\rm N})_{\rm c} = 4.87$–$7.19 \times 10^{-3}$ (Arpigny et al. 2003; Jehin et al. 2004, 2006, 2008; Hutsemékers et al. 2005; Bockelée-Morvan et al. 2008a, 2008b; Manfroid et al. 2009). In our models, we consider $(^{15}{\rm N}/^{14}{\rm N})_{\rm c}$ values in the range of 5.00–7.00 $\times$ 10^{-3}.

The current isotopic ratio of nitrogen in the Earth's atmosphere is $(^{15}{\rm N}/^{14}{\rm N})_{\rm t} = 3.676 \times 10^{-3}$. The blue line in Figure 3 shows that about 3%–8% of the Earth's atmospheric nitrogen was delivered by comets if no other processes changed the isotopic ratio since the comets were delivered. However, this current-day isotopic ratio may be lower that of the Archean atmosphere that reflects the effect of the late heavy bombardment (LHB). Nitrogen content of the Archean atmosphere was brought to subduction zones (Mallik et al. 2018) and it results in the current isotopic ratio of nitrogen in the Earth's atmosphere.

If we consider the higher isotopic ratio of nitrogen in Archean Earth's atmosphere of $(^{15}{\rm N}/^{14}{\rm N})_{\rm t} = 3.786 \times 10^{-3}$ (Jia & Kerrich 2004), the yellow line in Figure 3 shows that about 6%–15% of the Earth's atmospheric nitrogen was delivered by comets.

In summary, if the isotopic ratio of nitrogen has not changed since the Archean era, the cometary contribution of nitrogen is only about 5%. On the other hand, if in the Archean era, the Earth has an enriched ^{15}N atmosphere, the cometary contribution of nitrogen may be about 10%.

4. Debris Disk Evolution

We now consider possible delivery mechanisms for nitrogen containing comets in the Kuiper Belt to collide with Earth. We

Table 1
The Apsidal Eigenfrequencies for Each of the Solar System Planets

Planet	Apsidal Eigenfrequency (g_i) (arcsec yr^{-1})
Mercury (Me)	5.46347
Venus (V)	7.35054
Earth (E)	17.2968
Mars (M)	17.9887
Jupiter (J)	3.72802
Saturn (S)	22.5375
Uranus (U)	2.70839
Neptune (N)	0.633873

first consider an analytic secular resonance model, and then we use *N*-body simulations to model the delivery of comets to the Earth.

4.1. Resonances in the Kuiper Belt

In the context of the Kuiper Belt, interior mean-motion resonances with Neptune generally produce scattering events from eccentricity excitations compared with exterior mean-motion resonances that provide resonant capture of debris (Beauge & Ferraz-Mello 1994). Thus, we narrow our investigation of a nitrogen transport mechanism to secular resonances rather than including mean-motion resonances, as there are no interior mean-motion resonances within the Kuiper Belt. There are two types of secular resonances, apsidal and nodal. An apsidal resonance excites eccentricity, while a nodal resonance excites inclination (Froeschle et al. 1991). Apsidal resonances are the most important secular resonances for transporting material to the Earth, as the comets remain in the orbital plane of the system's solid large bodies with an increased eccentricity and are more likely to collide with the Earth. Here, we apply a first-order secular resonance model to the solar system to find all of the apsidal resonance locations. We are particularly interested in secular resonances that are outside of the ammonia snow line (at around 9 au at the end of the gas disk lifetime; see Section 2) as objects outside of this location may contain large amounts of nitrogen.

A secular resonance arises when the free precession rate of a test particle is equal to the eigenfrequency of one of the planets (e.g., Froeschle & Scholl 1986; Yoshikawa 1987; Minton & Malhotra 2011; Smallwood et al. 2018a, 2018b). The planetary eigenfrequencies are obtained by calculating the eigenvalues from the Laplace–Lagrange equations in the context of the generalized secular perturbation theory (see, for example, Murray & Dermott 1999). The eigenfrequencies for each of the solar system planets are shown in Table 1. The free precession rate of a test particle with orbital frequency, n, and semimajor axis, a, in the potential of the solar system is

$$\dot{\omega} = \frac{n}{4}\sum_{j=1}^{N}\frac{m_j}{m_*}\alpha_j\bar{\alpha}_j b_{3/2}^{(1)}(\alpha_j) \tag{27}$$

(Murray & Dermott 1999), where m_j is the mass of the solar system planets, m_* is the mass of the Sun, $b_s^{(j)}$ is the Laplace coefficient, and the coefficients α_j and $\bar{\alpha}_j$ are defined as

$$\alpha_j = \begin{cases} a_j/a, & \text{if } a_j < a, \\ a/a_j, & \text{if } a_j > a, \end{cases} \tag{28}$$

and

$$\bar{\alpha}_j = \begin{cases} 1, & \text{if } a_j < a, \\ a/a_j, & \text{if } a_j > a. \end{cases} \tag{29}$$

The top panel of Figure 4 shows the eigenfrequencies of the planets as horizontal dashed lines. The test particle free precession rate is represented by the solid lines. Where the solid lines cross a horizontal line there is an apsidal secular resonance.

We now consider the strength of the apsidal resonances. In the bottom panel of Figure 4, we show the forced eccentricity of a test particle in the solar system (for details on these calculations see Murray & Dermott 1999 and Minton & Malhotra 2011). Planetary debris that falls within the high eccentricity parts of the gray shaded regions undergoes eccentricity growth that leads to ejection or collision with a larger object. In the context of nitrogen transport to the Earth, the source of nitrogen may originate from the Kuiper Belt, which extends roughly from 30 to 50 au (Duncan et al. 1995). The ν_8 secular resonance is the most prominent secular resonance within the Kuiper Belt (Froeschle & Scholl 1986). It is produced when the free precession rate of the comets is close to the eigenfrequency of Neptune. According to our linear secular resonance model, the ν_8 resonance is located at 40.9 au (the resonance location is based on first-order approximations), which is consistent with the actual location of the resonance (Nagasawa & Ida 2000).

Populations of Kuiper Belt objects that are in resonance suggest that Uranus and Neptune underwent outward migration (Fernandez & Ip 1984; Malhotra 1993, 1995; Hahn & Malhotra 1999, 2005; Chiang & Jordan 2002; Chiang et al. 2003; Murray-Clay & Chiang 2005; Tsiganis et al. 2005; Morbidelli et al. 2007; Nesvorný 2015; Nesvorný & Vokrouhlický 2016). During this dynamical phase, resonant bodies in the Kuiper Belt were destabilized and there was a sudden massive delivery of planetesimals to the inner solar system (e.g., Levison & Morbidelli 2003; Gomes et al. 2005; Nesvorný et al. 2017). In particular, the ν_8 secular resonance swept through the inner parts of the Kuiper Belt (Nagasawa & Ida 2000) and caused a large fraction of the comets to acquire free precession frequencies similar to that of Neptune. Comets that originated or got "bumped" into this sweeping resonance would have undergone increased eccentricity excitations leading to collisions with Earth, allowing for the transport of nitrogen.

4.2. N-body Simulations of Earth Impacts

To study the delivery of comets to the Earth, we use the *N*-body simulation package, REBOUND, to model the Kuiper Belt including the Earth, the four giant planets, and the Sun in the solar system (Rein & Liu 2012). We use a hybrid integrator called *mercurius*. This integrator uses WHFast, which is an implementation of a Wisdom–Holman symplectic integrator to simulate the long-term orbit integrations of the planetary system. For close encounters of test particles and planets, it switches smoothly to IAS15, which is a 15th-order integrator, to simulate gravitational dynamics (Rein & Spiegel 2015; Rein & Tamayo 2015). Thus, we can calculate the evolution of the Kuiper Belt for a duration of one hundred million years (Myr) quickly and precisely. In our simulation, we take a snapshot every 0.1 Myr.

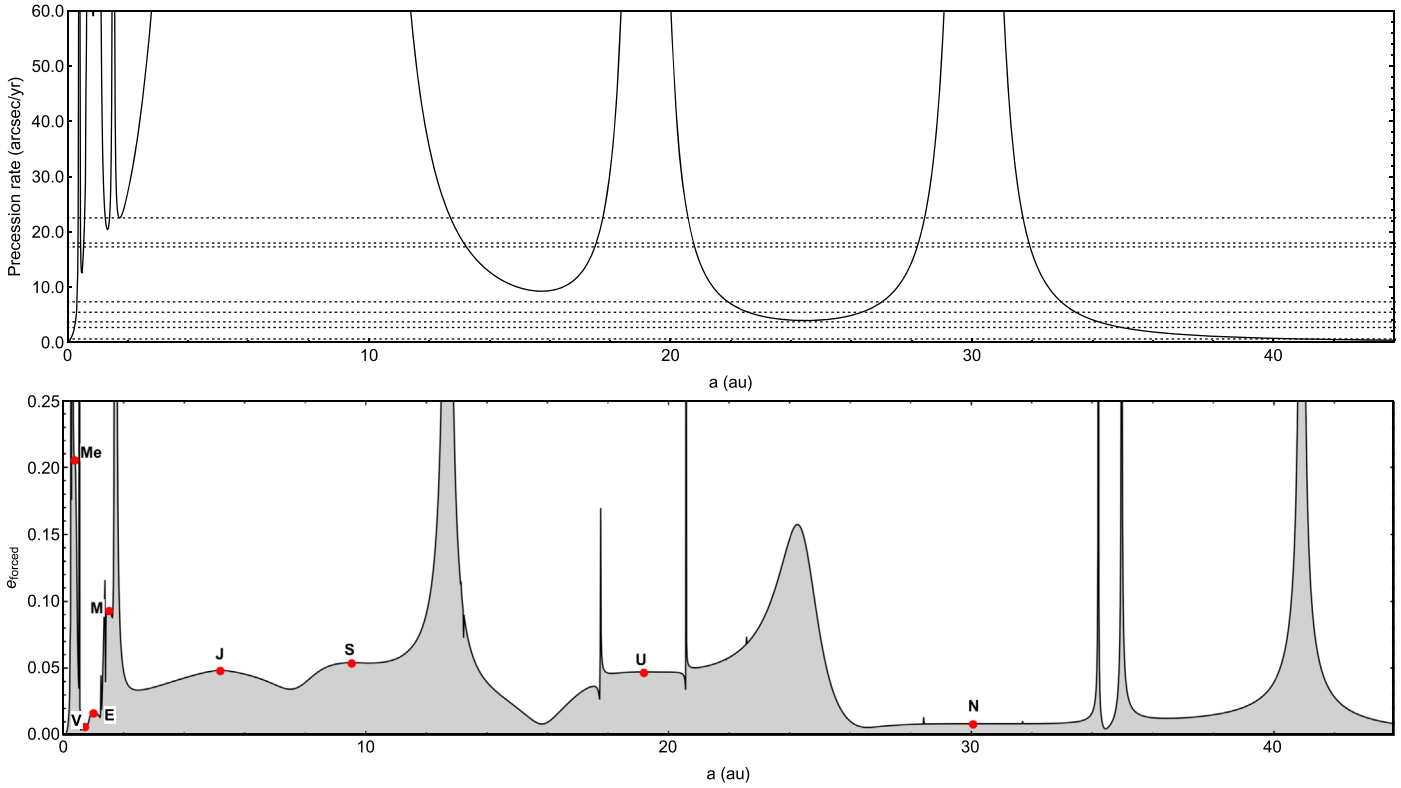

Figure 4. Top panel: the apsidal precession rate of a test particle as a function of semimajor axis (solid lines) and the eigenfrequencies for the planets (horizontal dotted lines; see Table 1 for specific values). The intersection of the test particle's precession rate with a planetary eigenfrequency represents the location of an apsidal secular resonance. Bottom panel: the maximum forced eccentricity of a test particle as a function of semimajor axis. The wider the gray region, the more asteroids/comets will undergo resonant perturbations.

Comets interact with the Earth, the gas giant planets, and the Sun due to gravitational forces, while there is no interaction between comets. The interaction timescale of some of the largest asteroids is of the order of magnitude of the age of the solar system (Dohnanyi 1969).

The obit of each comet is defined initially by six orbital elements, a, i, e, ω, Ω, ν. In our model, we assume the semimajor axis, a, is distributed uniformly in the range of $a_{\rm min} = 38$ to $a_{\rm max} = 45$ au, including the region of the ν_8 secular resonance (see Figure 4). The uniform distribution is given by

$$a_{\rm comet} = (a_{\rm max} - a_{\rm min}) \times \chi_r + a_{\rm min} \tag{30}$$

(Lecar & Franklin 1997; Smallwood et al. 2018a), and $\chi_{\rm r}$ is a randomly generated number between 0 and 1. The inclination, i, is randomly allocated in the range from 0° to 10° and the eccentricity, e, is randomly allocated in the range from 0 to 0.1. The argument of periapsis, ω, the longitude of the ascending node, Ω, and the true anomaly, ν, are all uniformly distributed in the range from 0° to 360°.

The present-day orbital elements for each of the planets are set as the initial parameters for the planets because the solar system is stable over long timescales (Duncan & Lissauer 1998; Ito & Malhotra 2006). REBOUND queries those data automatically from the NASA HORIZONS database. A test particle that has a semimajor axis beyond 200 au is considered to be ejected.

In our simulation, we inflate the size of the Earth to its Hill radius. The Hill radius is given by

$$R_{\rm H} = a_{\rm p}\left(\frac{M_{\rm planet}}{3M_{\odot}}\right)^{1/3}, \tag{31}$$

where $M_{\rm planet}$ is the mass of the planet and $a_{\rm p}$ is the semimajor axis of the planet (Delsanti & Jewitt 2006). The Hill radius for the Earth is 2×10^6 km. In principle, 3 Hill radii is the range of the planet's gravitational force, and comets cannot remain on stable orbits within this region (Gladman 1993; Chatterjee et al. 2008; Morrison & Malhotra 2015). The increased size of the Earth artificially increases the rate of collisions with the Earth, allowing us to simulate fewer particles than would have been present in the early Kuiper Belt.

Figure 5 shows the initial eccentricity and semimajor axis distribution of 50,000 test particles. There are a total of 104 test particles that collide with the Earth within 100 Myr, and the initial conditions for these are shown by the blue dots. Seventy of these test particles originate from the region of the ν_8 resonance around 40–42 au. The 3:2 and 5:3 mean-motion resonances of Neptune that are at 39.5 and 42 au also contribute a few of the collisions with the Earth.

On the other hand, a test particle that has a semimajor axis $a > 43$ au is quite stable, the region is regarded as having classic Kuiper Belt objects, and the final distribution of eccentricity and semimajor axis of the comets in Figure 6 is roughly consistent with that observed for Kuiper Belt objects. However, there are still many particles in the inner region where $a < 40$ au. Current observations show that this region is

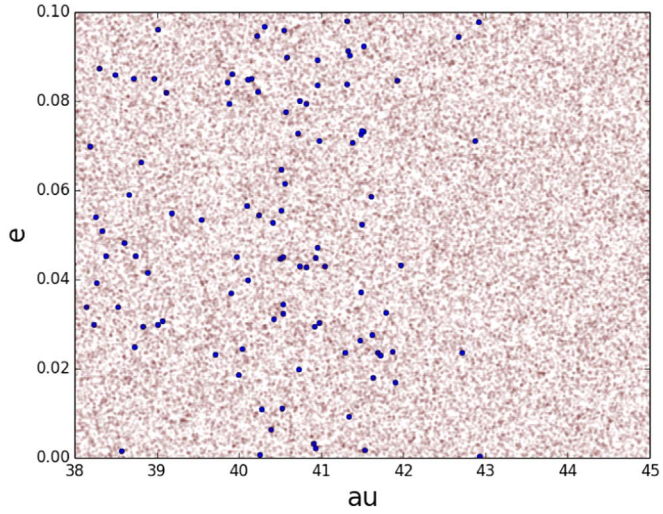

Figure 5. Initial distribution of semimajor axis and eccentricity of 50,000 test particles. Blue dots are particles that collide with the Earth.

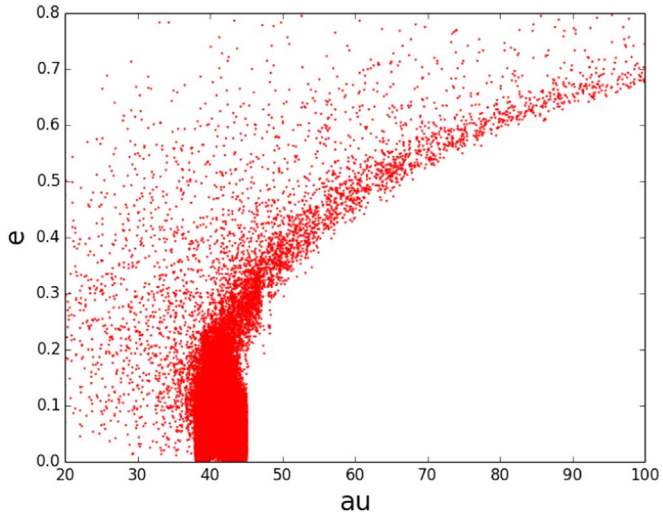

Figure 6. Final distribution of semimajor axis and eccentricity of the test particles that remain in the simulation.

quite clear (see Figure 7 in Jewitt et al. 2009). As we do not consider the outward migration of Uranus and Neptune in our simulation, we do not reproduce this clearing. The region of the ν_8 resonance is not completely cleared out of comets yet. About 50% of the test particles that were initially distributed in the region of the ν_8 resonance are still in this region.

Resonances in the Kuiper Belt excite the eccentricities of the test particles and this increases the chance of a close encounter with a planet. These close encounters result in outward or inward migration of test particles. Once a test particle comes into the inner solar system, the Earth has an opportunity to capture it. Figure 7 shows that particles begin colliding with the Earth after about 25 Myr, and there are more than four impact particles every 5 Myr after 30 Myr. In the next section, we use the results of our *N*-body simulation to estimate the amount of nitrogen that was delivered to the Earth from the Kuiper Belt.

4.3. Nitrogen Delivery to the Earth

We now consider a simple calculation to scale our simulation result to calculate how much mass may have been delivered to

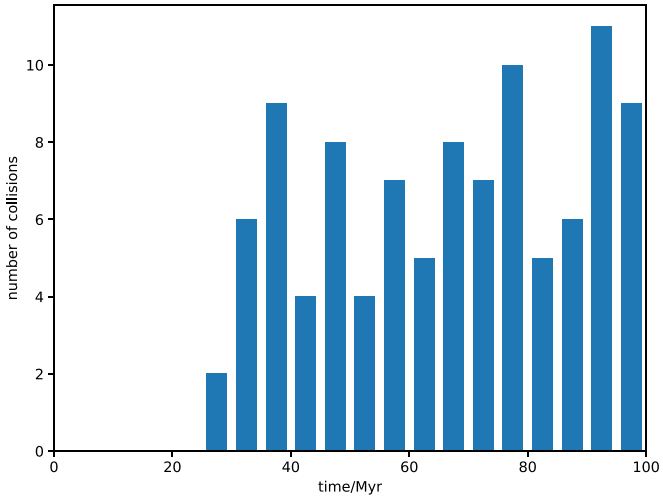

Figure 7. Histogram of the number of collisions of comets with the Earth as a function of time. There are 104 impact particles within 100 Myr.

the Earth by comets. Most of the impacts come from the ν_8 resonance region and we focus on these. The particles that begin in the region we are interested in, 40–42 au, assume a uniform distribution of the number of test particles in semimajor axis. However, we inflated the size of the Earth to increase the possibility of a collision. Smallwood et al. (2018a) calculated that the number of collisions is reduced by a factor of 800/5 if we shrink the size of the Earth from its Hill's radius to the radius of the Earth. Thus, the collision fraction should be 3×10^{-5} collisions per particle per 100 Myr.

The initial mass of the Kuiper Belt was at least 10 times the mass of Earth, $M_\oplus = 6 \times 10^{27}$ g (Delsanti & Jewitt 2006). The amount of mass that originated in the ν_8 resonance and collided with the Earth is approximately 5×10^{23} g in 100 Myr. Because at the end of our simulation there are still 50% of the original particles in the region of the ν_8 resonance, we multiply the number of collisions by a factor of 2 to find the mass to be $\approx 1 \times 10^{24}$ g. For comparison, the total mass that was delivered to the Earth during LHB is estimated to be around 2×10^{23}–2×10^{24} g by modeling the thermal effects of the LHB (Abramov et al. 2013). However, according to the constraint of atmospheric ^{36}Ar, Marty et al. (2016) estimated the cometary contribution to be about 2.0×10^{22} g. This value is 2 orders of the magnitude lower than our estimate. However, we have not taken into account the fact that a comet starts to sublime volatile when it enters the inner solar system. For example, the dynamical lifetime of the comet Halley is about 3000 perihelion passages or 0.2 Myr (Olsson-Steel 1988). It has lost about 0.4% of the total mass of the nucleus over the last 2200 yr (Schmude 2010). From observations, we have already found some small comets that have a radius <0.4 km that have lost of most their mass (see Table 9.4 in Fernández 2006). If we consider a comet that has a nucleus radius of 1 km, the bulk density is 0.5 g cm^{-3} and the perihelion distance is 1 au, and the dynamical lifetime is less than 1000 orbits (see Figure 9.2 in Fernández 2006). Due to the mass loss of comets, comets only possess 1% to 10% of their original mass when they collide with the Earth. Thus, the mass delivered by comets in our model is in the approximate range of 10^{22}–10^{23} g.

To calculate how much nitrogen could have been delivered in these comets, we use data of 16 comets from Le Roy et al. (2015) and Paganini et al. (2012) to estimate the mean values of

the highest relative abundances of NH_3 and HCN to be 0.7% and 0.28% with respect to water. Besides, in a recent study, ROSINA measured the N_2/CO ratio by mass to be 0.570% on the comet 67P/Churyumov–Gerasimenko, and CO in this comet is about 10% with respect to water (Le Roy et al. 2015). Thus, we use 0.057% for the relative abundance of N_2 with respect to water. H_2O takes up 50% of the composition of the comet by mass, and thus the total mass of nitrogen from comets is estimated to be in the range of 3.9×10^{19}–3.9×10^{20}g.

The total mass of the Earth's atmosphere is 5.136×10^{21}g (Weast et al. 1989). Nitrogen makes up 78% of the composition of the current Earth's atmosphere so that the mass of nitrogen in the atmosphere is 3.8×10^{21} g (Verniani 1966). If 10% of nitrogen was delivered by comets (see Section 3), the mass of cometary nitrogen is 4×10^{20}g, and our simulation is consistent with this value.

Note also that here we only consider the contribution from the ν_8 region. There would have been additional collisions as a result of mean-motion resonances of Neptune (see Figure 5) and the migration of Uranus and Neptune, which we did not include in our simulation. In the Archean era, the partial pressure of nitrogen was at least 1.4 $\sim$ 1.6 times higher than today's atmosphere. Mallik et al. (2018) estimated this value by subtracting the net degassing flux of N from arcs and back-arc basins (Hilton et al. 2002), mid-ocean ridges and intraplate settings (Sano et al. 2001) from the influx of N at subduction zones today. Due to N recycling efficiency, some nitrogen in the Earth's atmosphere was brought to the subduction zones and the deep mantle (Mallik et al. 2018). However, there are some contradictory results that the partial pressure of the nitrogen in Archean atmosphere is similar or less than the present atmosphere's based on different analyses of Archean samples (Som et al. 2016; Avice et al. 2018). Consequently, it leaves some uncertainties, and our simulations cannot solve this problem.

4.4. Water Delivery to the Earth

Because comets also contain a large amount of water, they deliver both nitrogen and water, and the D/H ratio in the Earth may also be changed. Since the D/H ratios of comets are much higher than terrestrial water and enstatite chondrites do not contain large amounts of water, it could be used to constrain the contribution of water from the comet to the Earth and it should be less than about 10% (Dauphas et al. 2000; Bockelée-Morvan et al. 2004). Since water takes up 50% of a comet's composition, we estimate the amount of water that was delivered from comets, and this value is $5 \times 10^{21} \sim 5 \times 10^{22}$ g. The total mass of the water on the Earth is 1.35×10^{24}g. Therefore, the water contribution from comets is just about 0.4% $\sim$ 4%. This value is more in agreement with Marty et al. (2016), who state the cometary contribution of water is $\leqslant$1%, whatever the reservoir considered.

5. Conclusions

Although it is not the main source of nitrogen in the Earth's atmosphere, a significant fraction of the present Earth's nitrogen may have come from comets (about 10%). The present isotopic ratio of $^{15}N/^{14}N$ in the Earth's atmosphere is a combination of the primitive Earth value and the value contained in asteroids/comets that hit the Earth. With steady-state protoplanetary disk models that include a self-gravitating dead zone, we find that the ammonia and nitrogen snow line radii were around 9 au and 12 au, respectively, at the end of the disk's lifetime. Thus, comets in the Kuiper Belt probably contain a large amount of nitrogen. Besides, the Kuiper Belt provides an extremely cold environment where CO is frozen out and large enhancements of the isotopic ratio $^{15}N/^{14}N$ occur there. Since the Earth's atmosphere might be enriched in ^{15}N in the Archean era, the nitrogen in the Kuiper Belt is a possible source.

Apsidal secular resonances played an essential role in bringing comets to the Earth. The most prominent secular resonance in the Kuiper Belt, the ν_8 resonance, might have excited the eccentricity of the comets. In the early stages of the solar system evolution, Uranus and Neptune both underwent outward migration during which the ν_8 resonance swept through comet-like objects from the inner Kuiper Belt to its present location at around 41 au. With numerical *N*-body simulations we have shown that comets around this region are scattered and may collide with the Earth when they enter the inner solar system. The period of the LHB corresponds with the early Archean era. During this time, the resonance most probably delivered comets and thus nitrogen to the Earth. With the supplement of the late delivery of nitrogen to the Earth, the isotopic ratio $^{15}N/^{14}N$ of the Earth's atmosphere increased slightly. Our research quantifies the amount of nitrogen that is delivered by comets.

Exoplanetary systems that contain both a warm and a cold debris belt (like the solar system) may be common (e.g., Moro-Martín et al. 2010; Morales et al. 2011). The outer debris disk is a potential source of nitrogen to terrestrial planets in the inner regions. For example, the planetary and debris disk system HR 8799 closely resembles that of the outer solar system by having two massive debris disks that bracket four giant planets, with the outermost disk consisting of cold dust ($T \sim 45$ K; Marois et al. 2008). Investigating the delivery of nitrogen in such systems can contribute to the understanding of the atmospheric properties of exoplanets and planetary habitability.

All the simulations were run at the UNLV National Supercomputing Institute on the Cherry Creek cluster. C.C. acknowledges support from a UNLV graduate assistantship. J. L.S. acknowledges support from a graduate fellowship from the Nevada Space Grant Consortium (NVSGC). R.G.M. acknowledges support from NASA grant NNX17AB96G. Simulations in this paper made use of the REBOUND code which can be downloaded freely at http://github.com/hannorein/rebound.

ORCID iDs

Cheng Chen https://orcid.org/0000-0002-4489-3491
Rebecca G. Martin https://orcid.org/0000-0003-2401-7168

References

Abramov, O., Kring, D. A., & Mojzsis, S. J. 2013, ChEG, 73, 227
Ader, M., Cartigny, P., Boudou, J.-P., et al. 2006, ChGeo, 232, 152
Armitage, P. J., Livio, M., & Pringle, J. E. 2001, MNRAS, 324, 705
Arpigny, C., Jehin, E., Manfroid, J., et al. 2003, Sci, 301, 1522
Avice, G., Marty, B., Burgess, R., et al. 2018, GeCoA, 232, 82
Bai, X.-N., & Goodman, J. 2009, ApJ, 701, 737
Balbus, S. A., & Hawley, J. F. 1991, ApJ, 376, 214
Balsiger, H., Altwegg, K., Bar-Nun, A., et al. 2015, SciA, 1, e1500377
Bar-Nun, A., Kleinfeld, I., & Kochavi, E. 1988, PhRvB, 38, 7749
Beauge, C., & Ferraz-Mello, S. 1994, Icar, 110, 239

Bergin, E. A., Blake, G. A., Ciesla, F., Hirschmann, M. M., & Li, J. 2015, PNAS, 112, 8965
Bockelée-Morvan, D., Biver, N., Jehin, E., et al. 2008a, ApJL, 679, L49
Bockelée-Morvan, D., Crovisier, J., Mumma, M. J., & Weaver, H. A. 2004, in Comets II, ed. M. C. Festou, H. U. Keller, & H. A. Weaver (Tucson, AZ: Univ. Arizona Press), 391
Bockelée-Morvan, D., Dello Russo, N., Jehin, E., et al. 2008b, LPICo, 1405, 8190
Bohlin, R. C., Savage, B. D., & Drake, J. F. 1978, ApJ, 224, 132
Cannizzo, J. K. 1993, ApJ, 419, 318
Cartigny, P., Harris, J., & Javoy, M. 1998, Sci, 280, 1421
Cartigny, P., & Marty, B. 2013, Eleme, 9, 359
Chatterjee, S., Ford, E. B., Matsumura, S., & Rasio, F. A. 2008, ApJ, 686, 580
Chiang, E. I., & Goldreich, P. 1997, ApJ, 490, 368
Chiang, E. I., & Jordan, A. B. 2002, AJ, 124, 3430
Chiang, E. I., Jordan, A. B., Millis, R. L., et al. 2003, AJ, 126, 430
Dauphas, N., Robert, F., & Marty, B. 2000, Icar, 148, 508
Delsanti, A., & Jewitt, D. 2006, in The Solar System Beyond The Planets, ed. P. Blondel & J. W. Mason (Berlin: Springer), 267
DeMeo, F. E., & Carry, B. 2014, Natur, 505, 629
Dohnanyi, J. S. 1969, JGR, 74, 2531
Duncan, M. J., Levison, H. F., & Budd, S. M. 1995, AJ, 110, 3073
Duncan, M. J., & Lissauer, J. J. 1998, Icar, 134, 303
Fernández, J. A. 2006, Comets: Nature, Dynamics, Origin, and their Cosmogonical Relevance, Vol. 328 (Springer Science & Business Media)
Fernandez, J. A., & Ip, W.-H. 1984, Icar, 58, 109
Froeschle, C., & Scholl, H. 1986, A&A, 166, 326
Froeschle, C., Scholl, H., & Morbidelli, A. 1991, A&A, 249, 553
Füri, E., & Marty, B. 2015, NatGe, 8, 515
Gammie, C. F. 1996, ApJ, 457, 355
Gammie, C. F., & Menou, K. 1998, ApJL, 492, L75
Garaud, P., & Lin, D. N. C. 2007, ApJ, 654, 606
Geiss, J. 1987, A&A, 187, 859
Geiss, J. 1988, RvMA, 1, 1
Gladman, B. 1993, Icar, 106, 247
Gomes, R., Levison, H. F., Tsiganis, K., & Morbidelli, A. 2005, Natur, 435, 466
Hahn, J. M., & Malhotra, R. 1999, AJ, 117, 3041
Hahn, J. M., & Malhotra, R. 2005, AJ, 130, 2392
Halliday, A. N. 2013, GeCoA, 105, 146
Harries, D., Hoppe, P., & Langenhorst, F. 2015, NatGe, 8, 97
Hayashi, C. 1981, PThPS, 70, 35
Hilton, D. R., Fischer, T. P., & Marty, B. 2002, RvMG, 47, 319
Hutsemékers, D., Manfroid, J., Jehin, E., et al. 2005, A&A, 440, L21
Hutsemékers, D., Manfroid, J., Jehin, E., & Arpigny, C. 2009, Icar, 204, 346
Ito, T., & Malhotra, R. 2006, AdSpR, 38, 817
Javoy, M. 1998, ChGeo, 147, 11
Javoy, M., Pineau, F., & Delorme, H. 1986, ChGeo, 57, 41
Jehin, E., Manfroid, J., Cochran, A. L., et al. 2004, ApJL, 613, L161
Jehin, E., Manfroid, J., Hutsemékers, D., et al. 2006, ApJL, 641, L145
Jehin, E., Manfroid, J., Kawakita, H., et al. 2008, LPICo, 1405, 8319
Jewitt, D., Moro-Martìn, A., & Lacerda, P. 2009, Astrophysics in the Next Decade (Berlin: Springer)
Jia, Y., & Kerrich, R. 2004, GGG, 5, 5
Johnson, B., & Goldblatt, C. 2015, Earth-Sci. Rev., 148, 150
Junk, G., & Svec, H. J. 1958, GeCoA, 14, 234
King, A. R., Pringle, J. E., & Livio, M. 2007, MNRAS, 376, 1740
Krankowsky, D. 1991, in Comets in the Post-Halley Era, ed. R. L. Newburn, Jr., M. Neugebauer, & J. Rahe (Dordrecht: Kluwer), 855
Lecar, M., & Franklin, F. 1997, Icar, 129, 134
Le Roy, L., Altwegg, K., Balsiger, H., et al. 2015, A&A, 583, A1
Levison, H. F., & Morbidelli, A. 2003, Natur, 426, 419
Lodders, K. 2003, ApJ, 591, 1220
Malhotra, R. 1993, Natur, 365, 819
Malhotra, R. 1995, AJ, 110, 420
Mallik, A., Li, Y., & Wiedenbeck, M. 2018, E&PSL, 482, 556
Manfroid, J., Jehin, E., Hutsemékers, D., et al. 2009, A&A, 503, 613
Marois, C., Macintosh, B., Barman, T., et al. 2008, Sci, 322, 1348
Martin, R. G., & Livio, M. 2012, MNRAS, 425, L6
Martin, R. G., & Livio, M. 2013, MNRAS, 434, 633
Martin, R. G., & Livio, M. 2014, ApJL, 783, L28
Martin, R. G., & Lubow, S. H. 2011, ApJL, 740, L6
Martin, R. G., & Lubow, S. H. 2013, MNRAS, 432, 1616
Martin, R. G., & Lubow, S. H. 2014, MNRAS, 437, 682
Martin, R. G., Lubow, S. H., Livio, M., & Pringle, J. E. 2012a, MNRAS, 420, 3139
Martin, R. G., Lubow, S. H., Livio, M., & Pringle, J. E. 2012b, MNRAS, 423, 2718
Marty, B. 1995, Natur, 377, 326
Marty, B. 2012, E&PSL, 313, 56
Marty, B., Altwegg, K., Balsiger, H., et al. 2017, Sci, 356, 1069
Marty, B., Avice, G., Sano, Y., et al. 2016, E&PSL, 441, 91
Marty, B., & Zimmermann, L. 1999, GeCoA, 63, 3619
Marty, B., Zimmermann, L., Pujol, M., Burgess, R., & Philippot, P. 2013, Sci, 342, 101
McKeegan, K. D., Aléon, J., Bradley, J., et al. 2006, Sci, 314, 1724
Meier, R., Eberhardt, P., Krankowsky, D., & Hodges, R. R. 1994, A&A, 287, 268
Minton, D. A., & Malhotra, R. 2011, ApJ, 732, 53
Morales, F. Y., Rieke, G. H., Werner, M. W., et al. 2011, ApJL, 730, L29
Morbidelli, A., Tsiganis, K., Crida, A., Levison, H. F., & Gomes, R. 2007, AJ, 134, 1790
Moro-Martín, A., Malhotra, R., Bryden, G., et al. 2010, ApJ, 717, 1123
Morrison, S., & Malhotra, R. 2015, ApJ, 799, 41
Murray, C. D., & Dermott, S. F. 1999, Solar System Dynamics (Cambridge: Cambridge Univ. Press)
Murray-Clay, R. A., & Chiang, E. I. 2005, ApJ, 619, 623
Murty, S. V. S., & Mohapatra, R. K. 1997, GeCoA, 61, 5417
Nagasawa, M., & Ida, S. 2000, AJ, 120, 3311
Nesvorný, D. 2015, AJ, 150, 73
Nesvorný, D., Roig, F., & Bottke, W. F. 2017, AJ, 153, 103
Nesvorný, D., & Vokrouhlický, D. 2016, ApJ, 825, 94
Notesco, G., & Bar-Nun, A. 1996, Icar, 122, 118
Oka, A., Nakamoto, T., & Ida, S. 2011, ApJ, 738, 141
Olsson-Steel, D. 1988, Exploration of Halley's Comet (Berlin: Springer), 909
Owen, T., & Bar-Nun, A. 1995, AIPC, 341, 123
Paganini, L., Mumma, M. J., Villanueva, G. L., et al. 2012, ApJL, 748, L13
Papineau, D., Mojzsis, S., Karhu, J., & Marty, B. 2005, ChGeo, 216, 37
Pinti, D. L., Hashizume, K., & ichi Matsuda, J. 2001, GeCoA, 65, 2301
Prialnik, D., & Bar-Nun, A. 1992, A&A, 258, L9
Pringle, J. E. 1981, ARA&A, 19, 137
Pringle, J. E., Verbunt, F., & Wade, R. A. 1986, MNRAS, 221, 169
Rafikov, R. R. 2015, ApJ, 804, 62
Rein, H., & Liu, S.-F. 2012, A&A, 537, A128
Rein, H., & Spiegel, D. S. 2015, MNRAS, 446, 1424
Rein, H., & Tamayo, D. 2015, MNRAS, 452, 376
Rice, T. S., Bergin, E. A., Jørgensen, J. K., & Wampfler, S. F. 2018, ApJ, 866, 156
Rodgers, S. D., & Charnley, S. B. 2008, MNRAS, 385, L48
Rubin, A. E., & Choi, B.-G. 2009, EM&P, 105, 41
Sano, T., Miyama, S. M., Umebayashi, T., & Nakano, T. 2000, ApJ, 543, 486
Sano, Y., & Pillinger, C. T. 1990, GeocJ, 24, 315
Sano, Y., Takahata, N., Nishio, Y., Fischer, T. P., & Williams, S. N. 2001, ChGeo, 171, 263
Schmude, R. 2010, Comets and How to Observe Them (Berlin: Springer)
Shakura, N. I., & Sunyaev, R. A. 1973, A&A, 24, 337
Smallwood, J. L., Martin, R. G., Lepp, S., & Livio, M. 2018a, MNRAS, 473, 295
Smallwood, J. L., Martin, R. G., Livio, M., & Lubow, S. H. 2018b, MNRAS, 480, 57
Som, S. M., Buick, R., Hagadorn, J. W., et al. 2016, NatGe, 9, 448
Stüeken, E., Buick, R., & Schauer, A. 2015, E&PSL, 411, 1
Stüeken, E. E., Kipp, M. A., Koehler, M. C., et al. 2016, AsBio, 16, 949
Toomre, A. 1964, ApJ, 139, 1217
Tsiganis, K., Gomes, R., Morbidelli, A., & Levison, H. F. 2005, Natur, 435, 459
Turner, N. J., & Sano, T. 2008, ApJL, 679, L131
Umebayashi, T., & Nakano, T. 1988, PThPS, 96, 151
Verniani, F. 1966, JGR, 71, 385
Wasson, J. T., & Kallemeyn, G. W. 1988, RSPTA, 325, 535
Weast, R. C., Astle, M. J., Beyer, W. H., et al. 1989, CRC Handbook of Chemistry and Physics (Boca Raton, FL: CRC press)
Wordsworth, R., & Pierrehumbert, R. 2014, ApJL, 785, L20
Wordsworth, R. D., & Pierrehumbert, R. T. 2013, ApJ, 778, 154
Yoshikawa, M. 1987, CeMec, 40, 233
Zhu, Z., Hartmann, L., Gammie, C. F., et al. 2010, ApJ, 713, 1134
Zhu, Z., Hartmman, L., Calvet, N., et al. 2007, ApJ, 669, 483